Journal of Engineering and Sustainable Development
Vol. 30, No. 04, July 2026
https://jeasd.uomustansiriyah.edu.iq/index.php/jeasd
ISSN 2520-0917
Research Article
https://doi.org/10.31272/jeasd.2567

Design and Simulation of a Sensor-less Pneumatic Dual-Axis Solar Tracking System in Baghdad City

Mustafa A. Abdul-Hussein[1*], Jamal A.-K. Mohammed[2], Wisam E. Abdul-Lateef[2], Amjad R. Mohammed[3]

[1]Air Conditioning and Refrigeration Techniques Engineering Department, College of Engineering, University of Warith Al-Anbiyaa, Karbala, Iraq
[2]Electromechanical Engineering Department, College of Electromechanical Engineering, University of Technology, Baghdad, Iraq
[3]College of Education for Humanities, University of Anbar, Iraq

[*]Email: mustafa.abbas3.142@gmail.com

Article Info

Received	**10/04/2024**
Revised	**03/06/2026**
Accepted	**06/06/2026**

Abstract

Fixed photovoltaic panels suffer from a major issue, which is low energy production due to their inability to track the sun. To solve this problem, these panels are installed on systems equipped with appropriate actuators to ensure they remain permanently aligned with sunlight during the day, thereby increasing solar radiation absorption. This paper aims to design and implement double-acting pneumatic actuators to steer a sensorless dual-axis solar tracking system under the worst climatic conditions. To achieve accurate tracking movement, the tracking angles were modeled in this system. The pneumatic solar system is designed using MATLAB/SIMSCAPE. Several tests were conducted under the worst weather conditions in Baghdad to collect data on the system model's input and output signals and evaluate its real-time performance. By modeling the system, specific pneumatic components can be selected to achieve the desired behavior by predicting and optimizing the performance of the pneumatic actuators under load. The results demonstrated that the analytical and simulation models agreed. The findings showed that when the solar panel was angled in two axes rather than a fixed panel, its efficiency increased by 56.4%.

Keywords: Dual-axis tracker, Photovoltaic panel, Pneumatic actuators, Rack and pinion gear, Wind

1. Introduction

Recently, sustainability has become increasingly important. Fossil fuels are losing ground to alternative energy sources [1]. Examples of these sources include wind and solar energy. Another increasingly appealing substitute for fossil fuels is solar energy. Air-heating devices [2], [3], water-heating devices [4], [5], crop-drying devices [6]-[7], producing electric energy [8], [9], irrigation systems [10], [11], etc. are only a few of the uses for solar energy. To meet growing electricity demand and achieve sustainability goals, a variety of methods are being employed, including solar, hydro, wind, and other renewable energy sources.

The increasing importance of renewable energy is driving up demand for solar energy equipment. Solar-powered systems are often utilized in residential, commercial, and agricultural settings. The solar panel of this device, which is driven by a solar tracking system and absorbs solar energy by aligning with the sun's position, is one of its most notable features [12], [13]. To ensure that the solar photovoltaic (PV) panels receive sunshine throughout the day, these products require the installation of solar tracking actuators. This makes it possible to position the solar panels as close to the sun as possible. These actuators help boost solar absorption when the sun is at a low angle.

Actuators are essential components of solar PV tracking systems; thus, their design must be carefully considered. Actuators must be incredibly robust, reliable, accurate, technically regulated, and compatible with solar trackers.

To improve the amount of sunlight hitting the photovoltaic cells and increase energy production, solar trackers monitor the sun's movement across the sky. A solar tracking system, combined with a PV panel driven by a geared motor or linear actuator, can achieve a 30–40% boost in panel efficiency compared with stationary panels [12]. Solar trackers frequently employ sensors and are driven by linear or rotary actuators [14]. These actuators allow for good tracking of sunlight.

Actuators may be driven by electric current or pressure (hydraulic or pneumatic). They convert energy into movement. The user can adjust the PV panel's angle. Based on the numerous structural degrees of freedom, PV tracking systems are classified into single-axis [15]-[17] and dual-axis [13], [18]. The azimuth angle is used in the first one to follow the sun along one axis, while the solar altitude and azimuth angles are used in the second one to track the sun along two axes. Both types of PV tracking systems have recently seen the development of new technologies and designs that provide remarkable control accuracy and structural dependability in real-world operation. The device's surface is constantly facing the sun, using a solar tracker to optimize energy capture. Stepper motors [17], direct current motors and gearboxes [19], [20], linear motors [21], [22], and stepper motor screwdrivers [23] are only a few more types of mechanical actuators. Further actuators, including hydraulic and thermomechanical ones [24], [25], can be employed to power the solar tracker. All previous research that used the aforementioned actuators to implement tracking mechanisms for solar tracking systems usually suffers from high cost, weight, control complexity, constant maintenance needs, and is not always suitable for all climatic conditions. Therefore, it was appropriate to invest in pneumatic actuators [26]-[28] to achieve the desired objective of the work.

Pneumatic actuators convert compressed air energy into mechanical energy for useful tasks. Stated differently, their purpose is to create displacement using the piston's movement or to provide the requisite force after the stroke. Pneumatic actuators are superior to hydraulic actuators in several ways [29]. They outperform hydraulic actuators in terms of manufacturing costs and resistance to contamination. Moreover, variations in external temperature have little effect on pneumatic actuator systems. Fluid pipes are not needed as actuator exhaust gases do not need to be collected. The pneumatic systems don't require long-term storage because they are nearly dry.

Pneumatic actuators frequently include a few essential features. For less money, they offer a better force/weight ratio. They demonstrate better positioning control, enhanced force control, and improved accuracy. These actuators are also more dependable, easier to operate, safer for workers, cleaner, more easily available, and more environmentally friendly than hydraulic controllers. Because of air compression, parasitic frictional effects, and nonlinear dynamics, pneumatic system designs [30] are substantially more challenging than those of other systems, despite their growing application.

Smooth, precisely regulated motion can be achieved by combining PV panel tracking systems with reliable, effective pneumatic actuators. Pneumatic actuators are an inexpensive way to change the height of a solar tracker. Because of its low-duty-cycle operation, the pneumatic tracker can monitor and scale potential while requiring less maintenance and using less energy. The solar tracker's actuators must be designed with flexibility, remarkable durability, reliability, and responsiveness in mind. Numerous industries and fields employ pneumatic actuators, including automotive [31], [32], lifting systems [33], tracking systems [26], [27], medical, robotics, and automation [34], etc.

There are very few papers in the literature concerning the topic of the present paper.

To boost energy consumption and reduce the corresponding losses, Al-Jaafari et al. [27] devised a closed-loop solar tracking system that is operated pneumatically. Accurate motion control was made possible by the rotating position sensor of the pneumatic cylinders, which also ensures very low consumption. The microcontroller controls rotation. With the closed pneumatic architecture, enhanced rotational and tilt inclination accuracy maximizes total stored energy and minimizes heat loss. To minimize energy consumption, the paper described the overall system components and their interactions.

In addition to adaptive shading, energy harvesting via sun-tracking is enabled by a continuously adjustable façade-shading system integrated with PVs. This necessitates significant bending in two directions. The creation of a suitable façade module, FlectoSol, was introduced by Born et al. [28]. For the first time, a GFRP-elastomer hybrid composite was integrated with two pneumatic actuators to achieve ±80 ° mobility. Parametric research was conducted to increase the use of actuation air pressure and energy efficiency without sacrificing shading. The impact of factors influencing the bending motion on the objective parameters was examined in detail. The laminate's overall stiffness limited the maximum bending angle to ±80°.

Fathi et al. [29] proposed a scalable design for a single-motor, dual-axis pneumatic solar tracker with fewer actuation switches and lower implementation costs. Taking into account the associated costs, the device uses Maximum Power Point Tracking (MPPT) to improve the PV system's actual efficiency. LDR sensors were used to drive the tracker in a closed-loop, dual-axis manner. The tracker offers low-duty-cycle operation with built-in energy storage, resulting in energy-efficient tracking, reduced maintenance requirements, and growth potential. The MPPT technology guarantees maximum power supply to the load. With an MPPT efficiency of 90%, the findings demonstrated a 37.6% increase in total power output and a 35.3% increase in real power output for the proposed tracking system compared to the fixed panel system.

Most papers in the solar tracking literature do not use pneumatic actuators to implement the tracking mechanism, nor do they employ a comprehensive calculation procedure when designing actuators across different climate scenarios. This study proposes the design and implementation of dual-acting pneumatic actuators to drive a dual-axis solar tracking system in the most adverse weather conditions. The objective of this study is to present a thorough design of the double-acting pneumatic actuators required to steer a sensorless dual-axis solar tracker, accounting for wind speed, impact angles, and the maximum allowable weight under the worst weather conditions in Baghdad. This sets it apart from the other related previous papers [27]-[29].

The internal piston diameters of two pneumatic cylinders and their stroke lengths were designed using MATLAB/SIMSCAPE simulation software to match the sun's daily and seasonal east-to-west and north-to-south excursions. The equations for the rack-and-pinion mechanisms were also

designed and implemented to convert the linear motion of one of the pneumatic cylinders into rotational motion in the tracking device. The proposed pneumatic solar tracker has several advantages over other tracking devices, as it is low-cost, environmentally friendly, easy to manufacture, requires no complex control circuits, and has low energy consumption.

The contribution of this work is also that the suggested off-line sensor-less dual-axis solar tracker tracks the sun's direction more accurately and has a much simpler structure than corresponding trackers reported in the literature [27]-[29], aside from sensor-based dual-axis solar trackers with expensive sensors mounted on highly accurate mechanical carriers. Furthermore, because the suggested tracker is offline and doesn't rely on a feedback signal, it is immune to external disruptions and meteorological conditions such as overcast skies, unlike all sensor-based solar trackers. The tracker determines the sun's direction that maximizes solar energy capture using offline-estimated data from solar map calculations.

2. Methodology

To implement the solar tracking mechanism, two double-acting pneumatic cylinders were constructed in this section to provide two degrees of freedom, along with rack-and-pinion mechanisms that convert one cylinder's linear motion into rotation. The first cylinder "1" is responsible for moving the solar panel from south to north. Its moving end is installed at one end of the panel's frame, while its other end is fixed to the pillar at a distance equal to one-third of the pillar's length, measured from its upper end. The second cylinder, "2," is mounted horizontally on the tracker base and rotates the pinion gear by half a revolution, thereby rotating the PV panel from east to west. The tracker's structure includes a frame for installing the panel, a pillar to raise the panel from the middle, and a base for mounting at the bottom. The frame is mounted on the pillar so that it can move freely. The rack gear is installed at the bottom of the pillar and transmits the movement from cylinder 2 to the pinion to generate the semicircular motion of the tracking system. The construction of the solar PV tracking system is illustrated in the diagram of Fig. 1.

In this design, a solar PV panel measuring 1340 × 850 × 20 mm and weighing 14 kg was used. A_p = 1340 × 850 mm is the area of the panel. The tracker features a 1460 mm-tall pillar and a 40 mm-diameter circular cross-section. A rectangular metal frame that matches the panel's size is used to install the PV panel using screws.

The MATLAB/SIMSCAPE simulation was used to model the pneumatic tracking system, assuming that the sun angles were the input and the pneumatic actuator displacement was the output.

The design of the pneumatic actuators that direct the PV panel toward the sun will be adopted in the following sections. This design is mainly based on calculating the set of maximum forces that hinder the movement of the actuators and other moving parts in the system. These forces are represented by weights and by the maximum wind forces expected in Baghdad's climate.

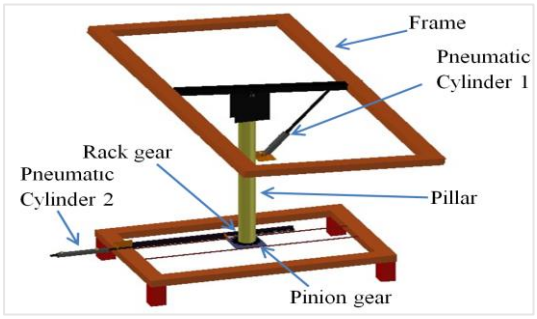

Figure 1. The complete structure of the two-axis solar tracker.

Due to variations in wind direction and composition, Iraq's wind energy distribution changes both regionally and temporally. Because of the country's exposure to several pressure systems, the work region experiences winds that fluctuate in speed and direction from one station to another throughout the year. Fig. 2 shows wind speed in Iraq at selected locations [35].

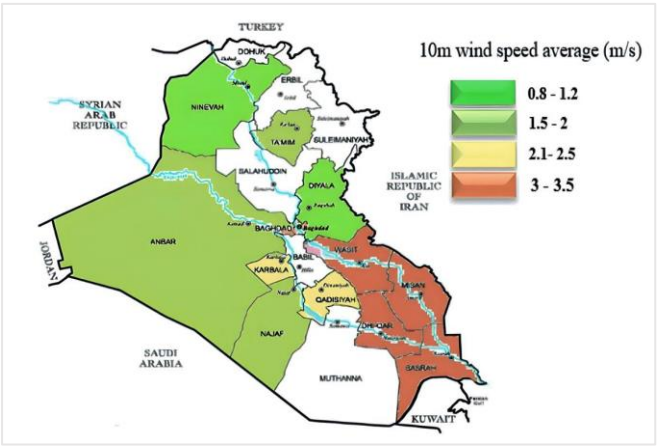

Figure 2. Map of wind speed at selected stations in Iraq [35].

In the Baghdad area, the average yearly wind speed might reach 3.5 m/s [35]. It was found that the wind map of Iraq created by the National Renewable Energy Center of Spain (CENER) and the generated wind map of average annual wind speed were quite close [36]. These data came from seismological surveys conducted across many Iraqi locales and from the Iraq Meteorological Organization.

2.1. Design of Pneumatic Cylinder 1

To track the sun's seasonal movement, one pneumatic cylinder must be designed to drive the PV panel from south to north. The PV tracking system's position for pneumatic cylinder 1 is shown in Fig. 1. The design involves determining safe values for the cylinder's length and diameter.

2.1.1. Designing the Length of Pneumatic Cylinder 1

The whole length of cylinder 1 (L_{C1}) when extended to the maximum distance (cylinder length + max stroke) may be computed using the Pythagorean theorem on the schematic seen in Fig. 3.

$$L_{C1}{}^2 = L_1{}^2 + L_2{}^2 - 2\,L_1 L_2\,cos(\theta) \quad (1)$$

Where L_1 = 425 mm is half the solar panel's width, L_2 = 486.7 mm is one-third of the pillar's length, and θ is the angle formed between the PV panel and the pillar. The pneumatic cylinder reaches its full stroke at θ = 90°. The tracking system's south-north rotation axis is positioned in the middle of the frame. Fig. 3 shows the minimum return and maximum expansion of the cylinder required for seasonal movement. By substituting the values of each variable into the equation, it was found that the value of LC1 is 646 mm. (The lengths of the cylinder's upper and lower holders, each measuring around 23 mm, must be removed from this length). To achieve the required angle, the stroke length of pneumatic cylinder 1 is (646/2) – 23 = 300 mm.

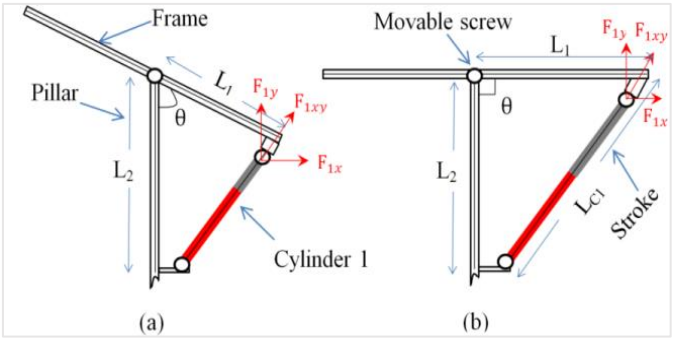

Figure 3. The pneumatic cylinder 1 with minimum returning (a) and maximum extension (b).

2.1.2. Designing the diameter of pneumatic cylinder 1

Calculating the diameter of pneumatic cylinder 1 initially requires determining the forces the cylinder must generate to push the required load.

The maximum force F_1 acting on cylinder 1 is equal to the sum of the force component F_{1y} perpendicular to the PV panel and the peak wind force F_w that faces the panel divided by sin θ.

$$F_1 = \frac{F_{1y}+F_w}{sin\,\theta} \quad (2)$$

$$F_{1y} = \frac{m}{2} \times g \times f \times c \quad (3)$$

$$F_w = A_W \times 0.5 \times \rho \times V^2 \times C_d \quad (4)$$

Where g = 9.8 m.s^{-2} is the acceleration caused by gravity, c is the bearing friction that was neglected because of the high air pressure. F is the surface friction that was disregarded since the surface area of friction is relatively small in comparison to the high air pressure, m = 15 kg is the PV panel's weight with its frame, C_d = 1.05 is the wind drag coefficient, A_W = 1340×850 mm^2 is the area of movable components facing the wind, V = 3.5 m.s^{-1} is the maximum speed of wind in Iraq country [36], and d ρ = 1.29 kg.m^{-3} is the air density. Around the middle of the frame, the panel weight is split equally between cylinder 1's two sides.

After executing the necessary calculations on the preceding equations, it was found that F_{1y} = 73.575 N. θ is chosen at 45° to provide the greatest lifting force [37]. From (4) [38], F_w = 9.45 N. Therefore, according to (2), the maximum total force acting on cylinder 1 is F_1 = 117.4 N.

The required pneumatic cylinder 1 diameter may be determined according to the following equations:

$$F_1 = A_1 \times P \quad (5)$$

$$A_1 = \frac{\pi}{4} \times D_1^2 \quad (6)$$

Where P is the cylinder air pressure (5 × 10 ^5 N/m^2), and A_1 is the area of cylinder 1. After calculating the A_1 value from (5), substituting it into (6), and using a safety factor of 1.5, the safe cylinder 1 diameter, D1, will be 26 mm.

2.2. Design of Pneumatic Cylinder 2

The linear movement of pneumatic cylinder 2 must be converted into rotational motion so the tracker can travel horizontally from east to west. This mechanism may be represented by a rack-and-pinion, as shown in Fig. 4.

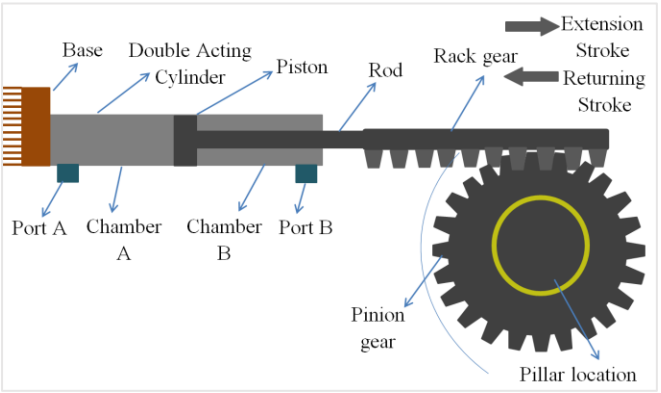

Figure 4. The mechanism responsible for the tracker movement from east to west

The pinion gear is installed at the bottom of the pillar. The rack gear is mounted horizontally on the base at the end of the cylinder to transmit its linear motion to the pinion, and, in turn, it is interlocked with the pinion gear to generate the pillar's rotational motion. The design of cylinder 2 involves finding safe values for its length and diameter.

2.2.1. Length design of the pneumatic cylinder 2

To simplify the design task, the pinion teeth and diameter were initially selected. The number of pinion teeth P_t= 62 and pinion diameter D_p= 124 mm.

It is worth noting that complete linear transmission of the rack requires the pinion disk to revolve half a revolution to accomplish a horizontal sweep of the PV panel from east to west. Making the rack's length equal to or larger than half the pinion's circumference accomplishes this. This will make meshing the gears simple and seamless.

$$R_l \geq \frac{Circumference\ of\ pinion}{2} = \frac{\pi\,D_p}{2} \quad (7)$$

The minimum rack length, Rl, is 194.78 mm. For design purposes, a rack length R_l of 250 mm was chosen, while the

stroke length of cylinder 2 was 200 mm. So, cylinder 2 will have a length of 220 mm and, fully extended, a length of 420 mm.

2.2.2. Designing the pneumatic cylinder 2

Using the previous equations and mechanical components, linear motion was converted into rotational motion, and the length of pneumatic cylinder 2 was set to 200 mm. Now here is a complete description of the design steps for calculating the diameter of the pneumatic cylinder 2.

It is possible to calculate the sum of the maximum forces (F_2) facing the movement of cylinder 2, which is the result of the sum of the weights of the moving parts (F_m) in addition to the maximum possible values of wind forces (F_w), as follows:

$$F_2 = F_m + F_w \quad (8)$$

F_m can be calculated based on Newton's second law of motion.

$$F_m = m \times g \times c \times f \quad (9)$$

Where m = 17 kg is the total mass of the moving components, including the solar panel with its frame (15 kg) and the pillar (2 kg); therefore, Fm was found to be 166.77 N. On the other hand, the maximum wind force F_w that can act on cylinder 2 is somewhat similar to that acting on cylinder 1.

As a result, the overall force acting on cylinder 2, according to (8), will be F_2 = 176.22 N.

The value of the required diameter D_2 of cylinder 2 can be derived from the area (A_2) of cylinder 2, which can be determined using the force equation:

$$F_2 = A_2 \times P \quad (10)$$

Substituting the air pressure $P = 5 \times 10^5$ N/m^2 in (10) to extract the cylinder area A_2. Substituting A_2 in (11) to find the cylinder diameter D_2:

$$A_2 = \frac{\pi D_2^2}{4} \quad (11)$$

Using a safety factor of 1.5, the designed value of D_2 will be 31.77 mm. All pre-designed parameters of pneumatic actuators are tabulated in Table 1.

The cylinders generate linear motion. Cylinder 2's linear motion is converted into rotational motion via a rack-and-pinion gear arrangement. Pneumatic control valves are used to manage system pressure, regulate airflow in pipes, and maintain a specific process temperature. Control signals are necessary for the regular opening and shutting of these valves. The mathematical model of the pneumatic system was simulated in MATLAB/SIMSCAPE to replicate the physical model closely. The valves must be controlled so that two normally closed valves are chosen. In this case, when electrical signals are applied to these valves, their positions are changed to always open, thereby controlling the movement of the corresponding cylinder. The pressure in chamber A must be equal to the pressure in chamber B. To move the cylinder forward, a control signal is sent to the second valve to open, releasing air from chamber B as the cylinder moves, and vice versa. Thus, the cylinder's movement can be controlled smoothly.

Table 1. Design parameters of pneumatic actuators.

Parameters	Actuator 1	Actuator 2
Cylinder stroke length (mm)	300	200
Cylinder internal diameter (mm)	26	31.77
Cylinder fully extended length (mm)	626	420
Cylinder fully retracted length (mm)	326	220
Force (N)	117.4	176.22
Rack length (mm)	-	250
Number of pinion teeth	-	62
Pinion diameter (mm)	-	124

3. Modeling of Pneumatic Tracking System

The overall pneumatic solar tracking system shown in Fig. 5 was modeled using MATLAB/SIMULINK. The system mainly consists of a PV solar panel, two double-acting pneumatic cylinders to guide the PV panel, a compressor, directional control valves, piping, and a rack-and-pinion gear system.

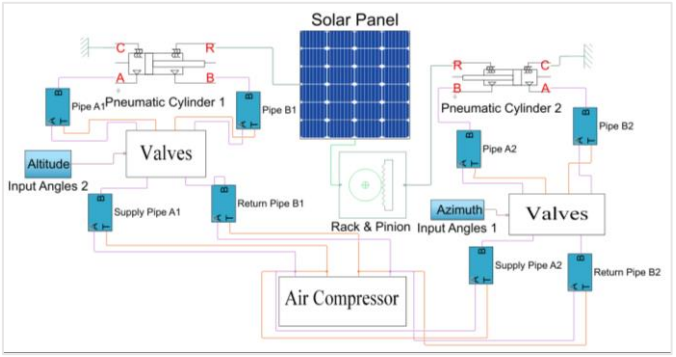

Figure 5. MATLAB/SIMSCAPE model of pneumatic tracking system.

The model also contains "Altitude" and "Azimuth" blocks for inserting the altitude and azimuth angles. The rotation angle of the tracking system in the vertical plane of space (θ_Z), i.e., the altitude angle, is calculated using the following formula [37]. An example of sun angles is shown in Fig. 6.

$$sin(\theta_Z) = \sin\varphi \sin\delta + \cos\varphi \cos\delta \cos\omega \quad (12)$$

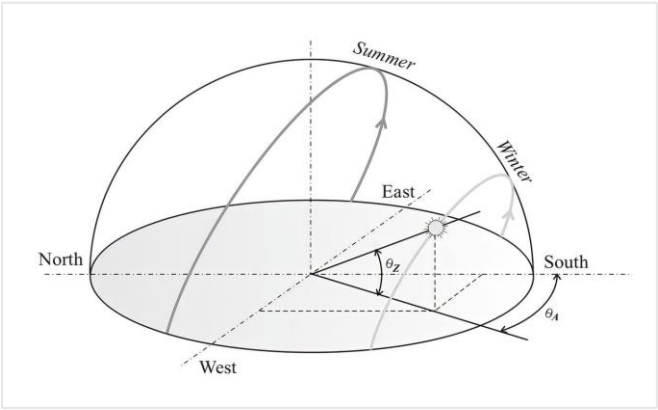

Figure 6. Standard behavior of the sun's path [38].

Where θ_Z is the system altitude angle, (θ_Z= 90°– sun zenith angle), φ is the latitude (φ = 33.34° for the case), ω =15°/h is the hour angle, using ω = 0 at local noon, and δ is the solar declination. δ can be found by the Cooper equation [38]:

$$\delta = 23.45\ sin\left[\frac{360}{365}\ (284 + N_d)\right] \qquad (13)$$

In this case, N_d = 1 denotes a single day of the year. It's April 1st, 2024. Conversely, the azimuth angle (θ_A), which denotes the rotational angle in the horizontal plane, is calculated as [38]:

$$sin(\theta_A) = \frac{cos(\delta)\ sin(\omega)}{cos(\theta_Z)} \qquad (14)$$

MATLAB/SIMSCAPE software was used to simulate the actual solar path at a latitude of 33.34°. Based on the solar declination (δ) of 6.85075° as displayed in Fig. 7, the simulation was conducted on April 1, 2024, on a bright day, to acquire azimuth-altitude angles in Baghdad city [39]. These angles are saved in a look-up table and can be extended to include all days of the year. Without the need for any sensors or feedback circuits, these angles may be recalled to drive the solar tracker offline.

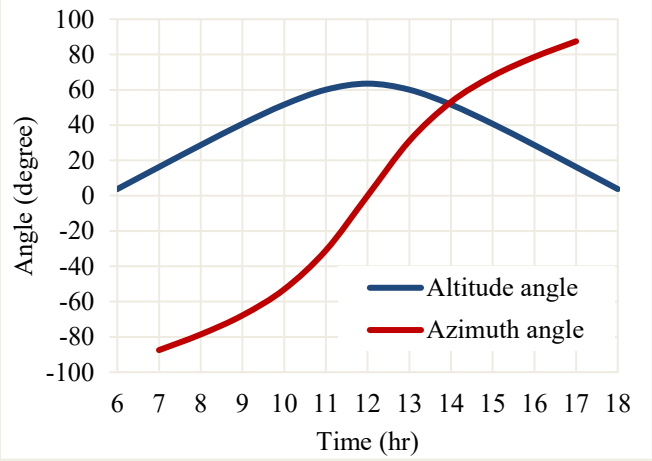

Figure 7. Azimuth-altitude angles during the 1st day of April 2024.

4. Simulation Results and Discussion

The MATLAB/SIMSCAPE software was used to implement the solar tracking system, driven by pneumatic actuators, to obtain a set of results. Tests were conducted on a sunny day on April 1, 2024, during which the ambient temperature varied as shown in Fig. 8. The temperature ranged between 12–24 °C from 6-11 am. The temperature remained nearly constant at 26 °C from 12:30 until 17:0, then began to decrease. Also, the figure depicts Baghdad's solar radiation on a day in April 2024.

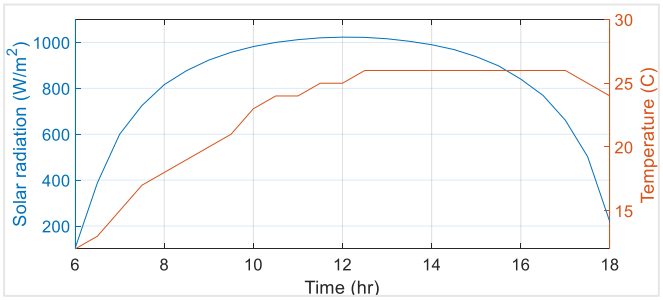

Figure 8. Ambient temperature and solar radiation during the 1st day of April 2024.

The air compressor's internal pressure and temperature are depicted in Fig. 9.

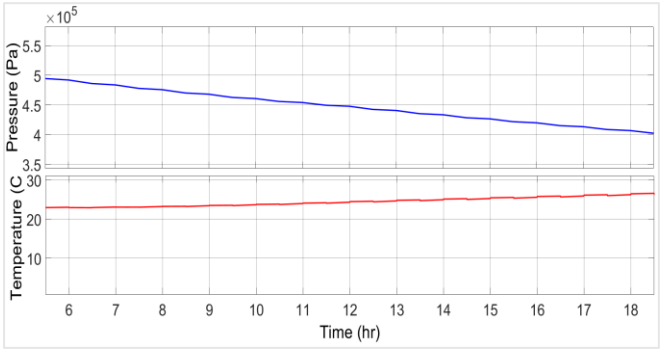

Figure 9. Internal compressor air pressure and temperature.

It is noted that the pressure decreases slightly and gradually, from 0.49 MPa at 6 o'clock to 0.41 MPa at 18 o'clock, while the temperature remains almost stable in the range of 22-25 °C. This indicates that the income system is stable.

The control valves receive hourly signals to control the piston position in the cylinder. Fig. 10 depicts the stroke displacement of cylinders 1 and 2 during the day. The cylinders ran from 6:00 to 18:00, reaching the greatest displacement strokes of 196 and 240 mm, respectively. The displaced position of the cylinders did not match the values of the stroke displacement shown in Table 1 because sunlight is not as perpendicular to the surface of the Earth in early spring (the current case study) as it is in summer. In design and calculations, this is taken into account to calculate the maximum angle during the year.

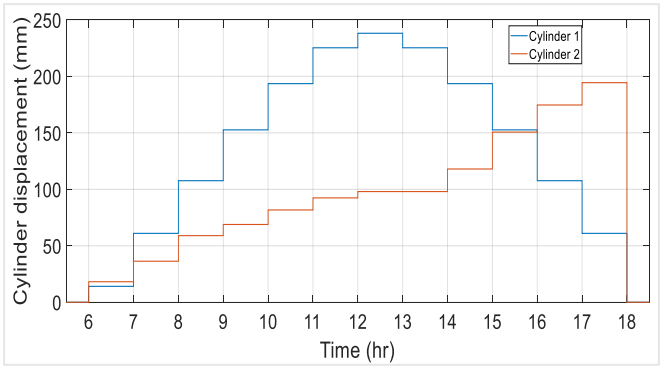

Figure 10. Stroke displacement of the pneumatic cylinders.

The scanning angles of the solar PV panels' daytime movement in the vertical and horizontal planes are depicted in Fig. 11.

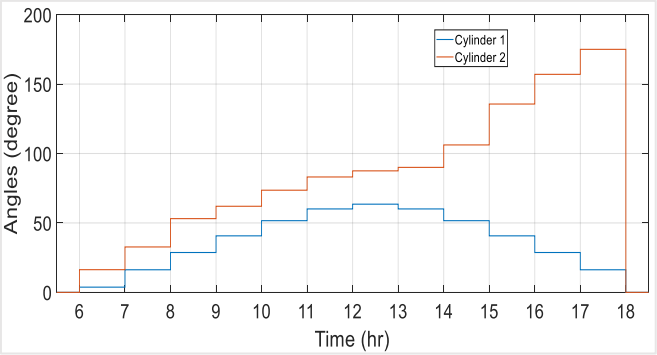

Figure 11. Vertical and horizontal scanning angles of the solar panel.

It is noted that the panel begins to rise vertically and gradually due to the action of cylinder 1, starting at 6:00 and continuing until midday, reaching a maximum scanning angle of 63.51° (1.108 rad), after which it descends and settles at the starting point at sunset.

Rack-and-pinion gears driven by pneumatic cylinder 2 cause the panel to rotate horizontally simultaneously, reaching its peak angle of 176.56 ° (3.08155 rad) at the end of the day.

The two pneumatic cylinders each come with two valves. This is done to sustain movement and apply pressure in two different directions. When the solar panel is tilted, the pressure in one of the cylinder chambers decreases, causing the panel to tilt toward the sun. Figs. 12 and 13 represent the pressures inside chamber A and chamber B of cylinders 1 and 2, respectively.

It is noted from Fig. 12 that the pressure at 6 o'clock inside chamber A is at its minimum, while it reaches a maximum inside chamber B, causing the piston to remain at the starting point and no displacement stroke to occur.

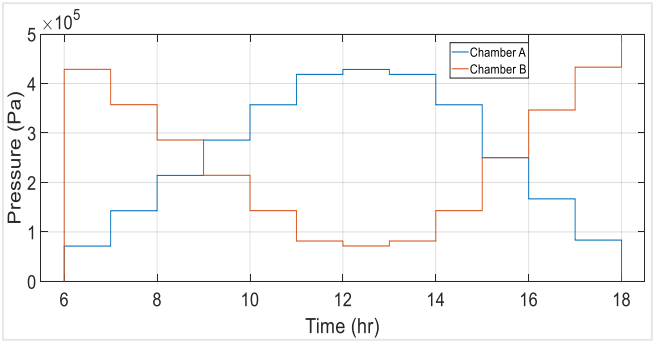

Figure 12. Pressures inside chambers of pneumatic cylinder 1.

When the sun rises, the pressure in chamber A gradually increases until it reaches its maximum at midday. At the same time, the pressure inside chamber B behaves exactly opposite to chamber A. After midday, the work of the chambers is exactly reflected, thus returning the cylinder stroke to its beginning, similar to the beginning of sunrise.

As for cylinder 2, Fig. 13 shows that the pressure inside chamber A is at its lowest at 6 o'clock, while it is at its highest in chamber B. This explains why there is no displacement stroke of the cylinder at this moment.

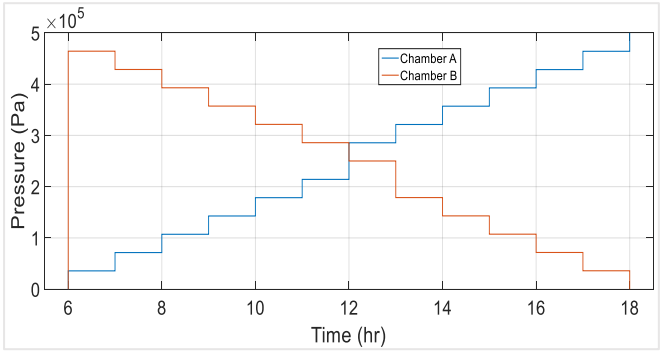

Figure 13. Pressures inside chambers of pneumatic cylinder 2.

After that, the pressure in chamber A gradually increases with sunrise, reaching its maximum at sunset (18 o'clock). Simultaneously, the pressure gradually decreases in chamber B until it reaches its minimum value at sunset. Through this mechanism, the stroke of cylinder 2 has shifted to its end. The pressures in chambers A and B are close to each other at midday, and cylinder stroke 2 is at the midpoint.

Fig. 14 represents the mass flow rate in cylinder 1 during the day. The air begins to flow from the compressor to chamber A at sunrise and exits chamber B into the tank. The process continues until midday, after which the process is reversed, with the flow from the compressor going to chamber B and exiting chamber A. This is due to the movement of the altitude angle, which rises from sunrise to midday and then decreases until sunset. For cylinder 2, Fig. 15 shows that the pressure in chamber A rises at sunrise to its maximum and remains stable until sunset, whereas the opposite occurs in chamber B. The mass flow rate increases as air flows from the compressor towards chamber A while exiting chamber B into the tank, causing the PV panel to move from east to west with the sun.

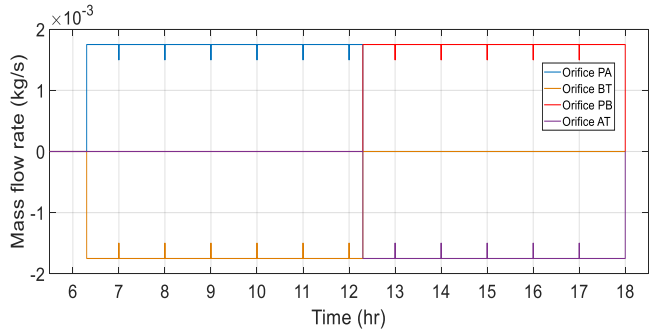

Figure 14. Mass flow rate in cylinder 1 during the day.

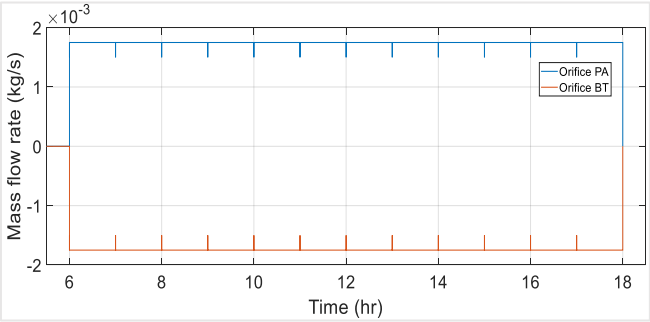

Figure 15. Mass flow rate in cylinder 2 during the day.

Where *PA* = Orifice *P* (air compressor) to Orifice *A* (chamber A), *PB* = Orifice *P* to Orifice *B* (chamber B), *BT* = Orifice *B* to Orifice *T* (Tank), and *AT* = Orifice *A* to Orifice *T*.

When the PV panel is loaded with a 50 Ω resistor, its output voltage and current can be multiplied to determine its output power (Po). Fig. 16 displays the distributions of the PV panel's output power when the panel is stationary or moving and following the sunlight. It can be found that the average power generated by a stationary solar panel and that for a mobile one with a tracking system are 63.98 W and 100.06 W, respectively. The figure shows that the power received from the movable panel remains at around 111.7 W from 7:00 to 17:30. In contrast, the power from the fixed panel increases gradually from the start of sunrise, reaching 109 W at midday and then dropping to 6 W, its lowest value, at sunset, after which it decreases gradually to reach 32.5 W at 18:30.

It is possible to draw the efficiency curves of the PV panel whether it is stationary or moving concerning the position of the sun, as shown in Fig. 17, depending on the wattage curves (Fig. 16) emerging from the panel, the area of the panel (A_p = 1.34×0.85 m^2), and the solar radiation intensity (G) curve (Fig. 8). The efficiency may be evaluated as:

$$\eta(\%) = \frac{P_o}{G\ A_p} \times 100\% \qquad (15)$$

It can be noted that the mobile panel's efficiency exceeds that of the fixed one during the day. The efficiency of the mobile panel reaches its highest value of 20.35% in the sunshine, then decreases until midday, and increases again until sunset. The situation is the opposite for fixed panels. It is found that the moving panel's average efficiency is 8.78%, whereas the fixed panel's average efficiency is 5.6%. This indicates that, compared with a fixed system, the tracking system increased PV panel efficiency by 56.4%.

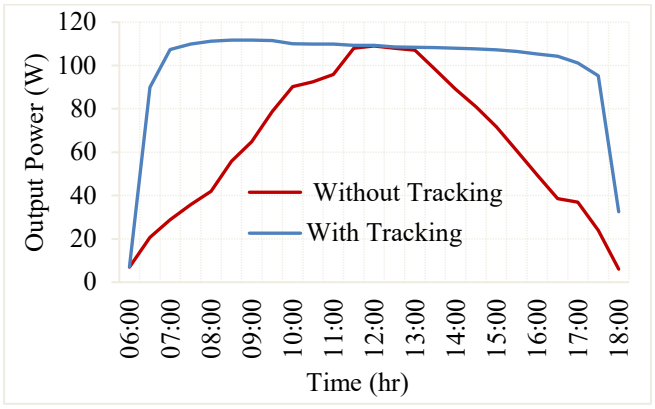

Figure 16. PV panel output power during the day.

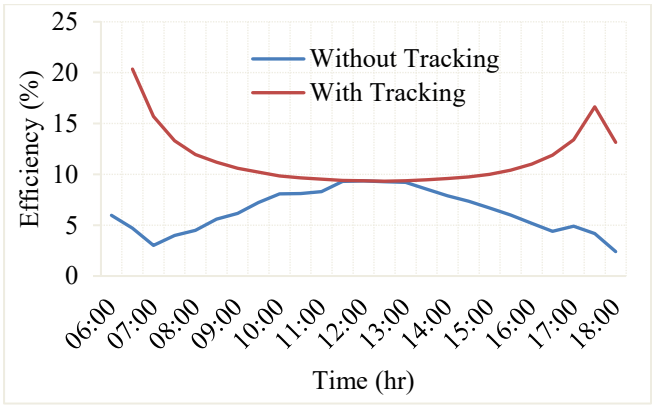

Figure 17. PV panel efficiency during daytime.

5. Conclusions

The objective of this paper is to design and implement dual-acting pneumatic actuators for a dual-axis solar tracking system, while operating under more adverse weather conditions under offline control. To keep the tracker up to date with the sun's daily and seasonal movement, air cylinders are designed with a suitable internal diameter and stroke length. Storing sun angles in a lookup table without sensors or feedback circuits, and calling them to steer the solar tracker in offline mode, enables the tracker to follow highly accurate paths. This, in turn, led to simplification and reduction in the cost of the control system. The proposed design of the pneumatic cylinders has enabled a quick, easy way to control the tracking system by precisely regulating the actuator's movement with respect to the sun's angles. The outcomes showed that there was agreement between the analytical models and the simulations made using a simulation tool. The findings demonstrated that the suggested operational model accurately represents the system's actual behavior. By accurately orienting the solar panel in two directions, pneumatic actuators increased its efficiency by 56.4% in comparison to a stationary panel. It is observed that during the start of sunrise and just before sunset, the suggested tracker may achieve the highest efficiency values.

It is a good idea to invest the electrical energy generated by solar panels in battery charging using MPPT charge controllers, thereby improving the performance of the solar tracker.

Acknowledgements

Many thanks and appreciation to the College of Electromechanical Engineering for providing the scientific environment to write this paper.

Conflict of interest

The authors declare that there are no conflicts of interest regarding the publication of this manuscript.

Author Contribution Statement

Mustafa A. Abdul-Hussein contributed to data organization, investigation, methodology, and statistical analysis.

Jamal A.-K. Mohammed contributed to conceptualization, supervision, modifications, and linguistic review.

Wisam E. Abdul-Lateef checked the results.

Amjad R. Mohammed provided guidance and support and checked the maps.

All authors discussed the results and contributed to the final manuscript.

References

[1] P. A. Owusu and S. Asumadu-Sarkodie, "A review of renewable energy sources, sustainability issues and climate change mitigation," *Cogent Engineering*, vol. 3, no. 1, no. 1167990, 2016. doi: https://doi.org/10.1080/23311916.2016.1167990.

[2] A. A. Ismaeel, H. A. Abdul Wahhab, and Z. H. Naji, "Performance evaluation of updraft air tower power plant integrated with double skin solar air heater," *Evergreen*, vol. 8, no. 2, pp. 296–303, Jun. 2021. doi: https://doi.org/10.5109/4480706.

[3] R. Kumar, S. K. Verma, N. K. Gupta, and S. K. Singh, "Performance enhancement of TSAH using graphene and graphene/CeO_2-black paint coating on absorber: A comparative study," *Evergreen*, vol. 9, no. 3, pp. 673–681, Sep. 2022. doi: https://doi.org/10.5109/4843098.

[4] Q. J. Abdul-Ghafoor, F. A. M. Abd Ali, W. K. Hasan, K. A. Hammoodi, and H. S. Majdi, "Enhancing thermal efficiency in solar water heaters using reflective mirrors," *International Journal of Design & Nature and Ecodynamics*, vol. 19, no. 1, pp. 31–39, 2024. doi: https://doi.org/10.18280/ijdne.190104.

[5] E. S. Barrak, K. A. Hammodi, and A. Mouthanna, "Thermal stratification in solar water storage tanks through inlet port diffuser optimization during charge and discharge processes," *Engineering Headway*, vol. 8, pp. 39–53, 2024. doi: https://doi.org/10.4028/p-1r0MVz.

[6] L. A. Rasheed, J. A.-K. Mohammed, and R. A. Jessam, "Performance enhancement of a single-pass solar air heater by adopting wire mesh absorber layer," *Evergreen*, vol. 10, no. 2, pp. 880–887, 2023. doi: https://doi.org/10.5109/6792883.

[7] L. A. Rasheed, J. A.-K. Mohammed, and R. A. Jessam, "Performance Enhancement of Solar Air Heater by Integrating Innovative Absorber Design and Automatic Control Flow Rate," *Evergreen*, vol. 10, no. 3, pp. 1439-1448, 2023. doi: https://doi.org/10.5109/7151693.

[8] A. Basem, M. Moawed, M. H. Abbood, W. M. El-Maghlany, "The design of a hybrid parabolic solar dish–steam power plant: An experimental study," *Energ Rep*, vol. 8, pp. 1949–1965, 2022. doi: https://doi.org/10.1016/j.egyr.2021.11.236.

[9] T. Hai, H. A. Jaffar, H. O. Shami, A. H. Al-Rubaye, H. Rajab, R. O. Farqad, A. H. A. Hussein, W. A. A. L. H. Alhaidry, A. H. Idan, and N. S. S. Singh, "Potential for on-grid hybrid renewable energy in a humid subtropical climatic zone: Technological, economic, and environmental aspects," *International Journal of Low-Carbon Technologies*, vol. 19, pp. 2409–2419, 2024. doi: https://doi.org/10.1093/ijlct/ctae196.

[10] W. H. Hassan and Z. N. Ghazi, "Assessing artificial recharge on groundwater quantity using wells recharge," *Civil Engineering Journal*, vol. 9, no. 9, pp. 2233–2248, 2023. doi: https://doi.org/10.28991/CEJ-2023-09-09-010.

[11] J. I. Herraiz, R. H. Almeida, M. Castillo-Cagigal, and L. Narvarte, "Experimental performance evaluation of a PV-powered center-pivot irrigation system for a three-year operation period," *Energies*, vol. 16, no. 9, no. 3654, 2023. doi: https://doi.org/10.3390/en16093654.

[12] H. S. Mahdi, "Design and Simulation of a 2 KVA PV Solar-Based Charge Control System," *Eng. Technol. J.*, vol. 33, no. 6 Part (A), 2015, https://uotechnology.edu.iq/tec_magaz/2015/volum332015/No.06.A.2015/Text(7).pdf

[13] A. Musa, E. Alozie, S. A. Suleiman, J. A. Ojo, and A. L. Imoize, "A review of time-based solar photovoltaic tracking systems," *Information*, vol. 14, no. 4, Art. no. 211, 2023. doi: https://doi.org/10.3390/info14040211.

[14] A. Awasthi, A. K. Shukla, S. R. M. Manohar, *et al.*, "Review on sun tracking technology in solar PV system," *Energy Reports*, vol. 6, pp. 392–405, 2020. doi: https://doi.org/10.1016/j.egyr.2020.02.004.

[15] S. Mirić, R. Giuffrida, G. Rohner, D. Bortis, and J. W. Kolar, "Design and experimental analysis of a self-bearing double-stator linear-rotary actuator," in *Proc. 2021 IEEE International Electric Machines & Drives Conference (IEMDC)*, 2021, pp. 1–8. doi: https://doi.org/10.1109/IEMDC47953.2021.9449501.

[16] M. J. Nahar, M. R. Sarkar, M. Uddin, M. F. Hossain, M. M. Rana, and M. R. Tanshen, "Single axis solar tracker for maximizing power production and sunlight overlapping removal on the sensors of tracker," *Int. J. Robot. Control Syst.*, vol. 1, no. 2, pp. 186–197, 2021. doi: https://doi.org/10.31763/ijrcs.v1i2.333.

[17] V. S. Qader, O. M. Ali, and N. I. Hasan, "An experimental comparison between fixed and single-axis tracking photovoltaic solar panel performance: Zakho City as case study," *Al-Rafidain Engineering Journal*, vol. 28, no. 1, pp. 272–279, Mar. 2023. doi: https://rengj.uomosul.edu.iq/index.php/rengj/article/view/30836

[18] N. Thungsuk *et al.*, "Performance analysis of solar tracking systems by five-position angles with a single axis and dual axis," *Energies*, vol. 16, no. 16, Art. no. 5869, 2023. doi: https://doi.org/10.3390/en16165869.

[19] H. Shang and W. Shen, "Design and implementation of a dual-axis solar tracking system," *Energies*, vol. 16, no. 17, no. 6330, 2023. doi: https://doi.org/10.3390/en16176330.

[20] P. Muthukumar, S. Manikandan, R. Muniraj, T. Jarin, and A. Sebi, "Energy-efficient dual-axis solar tracking system using IoT," *Measurement: Sensors*, vol. 28, no. 100825, 2023. doi: https://doi.org/10.1016/j.measen.2023.100825.

[21] K. J. Alaameri, A. J. Ramadhanand, and A. S. Maklakov, "Design of dual-axis solar tracking system with integrated cleaning system: Case study of Najaf city, Iraq," *AIP Conference Proceedings*, vol. 2386. no. 050001, 2022. doi: https://doi.org/10.1063/5.0066840.

[22] H. Asyari and A. W. Aji, "Desain solar tracking dual axis berbasis Arduino dan sensor light-dependent resistor untuk meningkatkan daya keluaran sel surya," *Jurnal Teknik Elektro UNIBA*, vol. 7, no. 2, pp. 320–324, 2023. doi: https://doi.org/10.36277/jteuniba.v7i2.218.

[23] S. E. Gun, L. Halim, and F. Wahab, "Solar panel efficiency improvement through dual-axis solar tracking with fuzzy logic and water treatment techniques," *Jurnal Nasional Teknik Elektro*, vol. 12, no. 3, pp. 20–29, 2023. doi: https://doi.org/10.25077/jnte.v12n3.1120.2023.

[24] J. K. Tharamuttam and A. K. Ng, "Design and development of an automatic solar tracker," *Energy Procedia*, vol. 143, pp. 629–634, 2017. doi: https://doi.org/10.1016/j.egypro.2017.12.738.

[25] A. Riad, M. Ben Zohra, A. Alhamany, and M. Mansouri, "Bio-sun tracker engineering self-driven by thermo-mechanical actuator for photovoltaic collectors," *Case Studies in Thermal Engineering*, vol. 21, Art. no. 100709, 2020. doi: https://doi.org/10.1016/j.csite.2020.100709.

[26] A. Abu Hanieh, "Fluid power control for sun tracking of solar panels: Modeling and simulation," *International Journal of Applied Mathematics, Electronics and Computers*, vol. 4, Special Issue, pp. 122–127, 2016. [Online]. Available: https://ijamec.org/index.php/ijamec/article/view/164.

[27] M. Jaafari, I. Hadachi, M. Elwarari, S. Boualila, and Y. Salih-Alj, "A closed pneumatic-based solar tracking system," in *Proc. 2013 International Renewable and Sustainable Energy Conference (IRSEC)*, 2013, pp. 136–140. doi: https://doi.org/10.1109/IRSEC.2013.6529725.

[28] L. Born, S. M. Gonzalez, A. Edith, M. Ridder, A. H. Körner, J. Knippers, and G. T. Gresser, "FlectoSol—A pneumatically activable PV-functionalized façade shading module with bending motion in two directions for solar tracking," *Developments in the Built Environment*, vol. 18, Art. no. 100372, 2024. doi: https://doi.org/10.1016/j.dibe.2024.100372.

[29] M. Fathi, R. Amjadifard, F. Eshghi, and M. Kelarestaghi, "Design and implementation of a novel multi-faceted-efficient pneumatic dual-axis solar tracker," *World Journal of Engineering*, vol. 21, no. 2, pp. 254–266, 2024. doi: https://doi.org/10.1108/WJE-04-2022-0173.

[30] J. Pustavrh, M. Hočevar, P. Podržaj, A. Trajkovski, and F. Majdič, "Comparison of hydraulic, pneumatic and electric linear actuation systems," *Scientific Reports*, vol. 13, Art. no. 20938, 2023. doi: https://doi.org/10.1038/s41598-023-47602-x.

[31] A. A. Mansour, W. M. Hashim, and A. A. W. Muhammad, "Design and implementation of a pneumatic servo system using conventional direction control valve," *Iraqi Journal of Computers, Communications, Control and Systems Engineering*, vol. 18, no. 3, pp. 1–11, 2018. doi: https://doi.org/10.33103/uot.ijccce.18.3.1.

[32] B. U. Okonkwo, M. C. Osuagwu, C. C. Chiabuotu, and K. C. Aladum, "Design analysis of a pneumatic vehicle," *Journal of Basic and Applied Research International*, vol. 29, no. 2, pp. 1–15, 2023. doi: https://doi.org/10.56557/JOBARI/2023/v29i28250.

[33] V. Patel, S. Shah, P. Shah, J. Patel, and S. Bhaduwala, "Experimental analysis of pneumatic vehicle: A research paper," *International Journal of Engineering Research & Technology*, vol. 6, no. 5, pp. 746–751, 2017. doi: https://www.ijert.org/experimental-analysis-of-pneumatic-vehicle-a-research-paper.

[34] S. Wakimoto, "F112006: Pneumatic soft actuators for medical applications," in *Proc. Mechanical Engineering Congress, Japan 2014*, 2014, pp. F112006-1–F112006-4. doi: https://doi.org/10.1299/jsmemecj.2014._F112006-1.

[35]B. Mohammed, O. I. Abdullah, and A. I. Al-Tmimi, "Investigation and analysis of wind turbines optimal locations and performance in Iraq," *FME Transactions*, vol. 48, no. 1, pp. 155–163, 2020. doi: https://doi.org/10.5937/fmet2001155B.

[36] A. K. Mishaal, A. M. Abd Ali, and A. B. Khamees, "Wind distribution map of Iraq—A comparative study," *IOP Conference Series: Materials Science and Engineering*, vol. 928, Art. no. 022044, 2020. doi: https://doi.org/10.1088/1757-899X/928/2/022044.

[37] Z. Gao, S. Zhou, J. Zhang, Z. Zeng, and X. Bi, "Parameterization of sea surface drag coefficient for all wind regimes using 11 aircraft eddy-covariance measurement databases," *Atmosphere*, vol. 12, no. 11, Art. no. 1485, 2021. doi: https://doi.org/10.3390/atmos12111485.

[38] A. Abu Hanieh, "Solar photovoltaic panels tracking system," in *Proc. 6th WSEAS International Conference on Dynamical Systems and Control*, Sousse, Tunisia, May 2010, pp. 30–37. [Online]. Available: https://dl.acm.org/doi/10.5555/1844329.1844336.

[39] M. S. Sachit, H. Z. M. Shafri, A. F. Abdullah, and A. S. M. Rafie, "Combining re-analyzed climate data and landcover products to assess the temporal complementarity of wind and solar resources in Iraq," *Sustainability*, vol. 14, no. 1, no. 388, 2022. doi: https://doi.org/10.3390/su14010388.